

# DIFFERENTIAL TOTAL ABSORPTIVITY SOLUTION TO THE RADIATIVE TRANSFER EQUATION FOR MIXTURES OF COMBUSTION GASES AND SOOT

*N. W. Bressloff, J.B. Moss, and P. A. Rubini*  
School of Mechanical Engineering, Cranfield University,  
Cranfield, Bedfordshire MK43 0AL, England

*The differential total absorptivity (DTA) solution to the radiative transfer equation, originally devised for combustion gases in the discrete transfer radiation model, is extended to mixtures of gaseous combustion products and soot. The method is compared to other solution techniques for representative mixtures across single lines of sight and across a layer bounded by solid walls. Intermediate soot loadings are considered such that the total radiance is not dominated by either the gaseous or soot components. The DTA solution is shown to yield excellent accuracy relative to a narrow-band solution, with a considerable saving in computational cost. Thus, explicit treatment of the source temperature dependence of absorption is successfully demonstrated without the need for spectral integration.*

## INTRODUCTION

Thermal radiation plays a crucial role in the coupling of combustion, heat transfer, and fluid dynamics in a wide range of combustion environments. Temperature changes due to radiation ultimately affect the yield of combustion products, and thence the concentrations of species and particulates influence the further emission, absorption, and scattering of radiation. Simultaneously, the fluid flow varies as a result of changes in **thermodynamic** properties, especially density. In enclosure fires, it is necessary to restrict rapid fire spread by retarding radiative energy transfer to combustible surfaces [1]. However, in furnaces it is desirable to optimize the radiant output from flames to increase the efficiency of furnace operation [2]. With respect to controlling combustor emissions, the very different and complex temperature dependencies of pollutant formation [3]—**particularly NO<sub>x</sub> and soot—require** a clear understanding of the radiative energy transfer accompanying these processes.

This initial discussion serves to highlight two critical aspects of accurate radiation modeling. First, it is necessary to **ascertain** the distribution of the major contributors to radiative exchange. In recent years, extensive research has been conducted into improved modeling of the distribution of combustion products, especially soot, in a range of combustion scenarios [4]. Second, the emission,

Received 7 March 1996; accepted 13 June 1996.

The support of EPSRC (Process Engineering Programme) for the research reported through Grant GR/H 80088 is greatly acknowledged.

Address correspondence to Dr. P. A. Rubini, School of Mechanical Engineering, Cranfield University, Cranfield, Bedfordshire MK43 0AL, England. E-mail: p.rubini@cranfield.ac.uk

Numerical Heat Transfer, Part B, 31:43–60, 1997

Copyright © 1997 Taylor & Francis

1040-7790/97 \$12.00 + .00

43

NOMENCLATURE			
$a_{m,n,n'}$	gray-gas polynomial weighting coefficient	$\tau$	transmissivity
$c_0$	constant in absorption coefficient for soot	$\omega$	soot volume fraction
$C_1, C_2$	Planck's first and second constants	Subscripts	
$E$	mean percentage absolute error	$b$	blackbody quantities
$i$	radiative intensity, $\text{kW}/\text{m}^2/\text{sr}$	$c$	carbon dioxide
$i_\nu$	spectral radiative intensity, $\text{kW cm}/\text{m}^2/\text{sr}$	$g$	gas
$k$	absorption coefficient, $\text{m}^{-1}$	$h$	water
$l$	path length, m	$i$	species
$N$	total number of cells in a path	$j$	spectral band or gray-gas component
$p$	partial pressure, atm	$m$	mixture
$q^-$	incident radiative flux, $\text{kW}/\text{m}^2$	$n, r, r'$	computational grid cell
$s, s', s''$	distance, m	$N$	final cell in path
$T$	temperature, K	$O$	origin of path
$T'_w$	effective wall temperature, K	$P$	soot
$a$	absorptivity	$s$	source temperature
$\Delta A$	area of a surface element, $\text{m}^2$	$v$	wave number
$e$	emissivity	Superscript	
$\lambda$	wavelength, m	$T$	total property
$\nu$	wave number, $\text{m}^{-1}$		
$\rho$	density, $\text{kg}/\text{m}^3$		
$\sigma$	Stefan-Boltzmann constant, $\text{kW}/\text{m}^2 \text{K}^4$		

scattering, and absorption characteristics of these components should be modeled at a level commensurate with that adopted for predicting their distribution. This second aspect characterizes the focus of the current article.

The differential total absorptivity (DTA) solution [5] to the radiative transfer equation (RTE) was originally devised to model the radiative properties of gaseous products of combustion. Bressloff et al. [5] demonstrated superior accuracy of the method relative to other approximate techniques when applied in the discrete transfer radiation model (DTRM) of Lockwood and Shah [6]. A more challenging test of the DTA solution is provided by mixtures of  $\text{CO}_2$ ,  $\text{H}_2\text{O}$ , and soot.

Unlike the banded nature of gaseous radiation, soot radiates in a continuous spectrum primarily in the visible and near-infrared. Consequently, the physics of gaseous and particulate radiation are very different [7]. These differences are manifested in existing solution techniques to the RTE.

In the statistical narrow-band model [8], the combined treatment of gaseous and particulate radiation is relatively straightforward in that banded transmissivities are simply the product of each component transmissivity. The method has been used successfully in the DTRM by Fairweather et al. [9], as described below. However, since the differential banded transmissivity (DBT) solution to the RTE, which employs narrow-band transmissivity data, solves an integral for every path for the hundreds of individual bands, the method is very computationally expen-

sive. Indeed, Fairweather et al. [9] performed the calculation only once as a **postprocess**. The exponential wide-band model [10] has proved more popular in the DTRM, since path integrals are required for over an order of magnitude fewer bands [11]. Felske and Tien [12], who applied the method to evaluate the total emissivity of luminous flames, demonstrated that there is an intermediate range of soot loading in which it is necessary to model the combined effects of gas and soot emission. Markstein [13] reached a similar conclusion following his experimental analysis of arrays of laminar flames with different propensities to soot.

Modak [14] also used the exponential wide-band model to establish a set of Chebyshev curve fits to total emissivity data. The total **emissivities** thus calculated for the gaseous mixture were then used by Grosshandler and Modak [15] in the total transmittance, nonhomogeneous (**TTNH**) model and combined with a direct solution to the RTE for soot, and a correction for overlap, to calculate the **line-of-sight** radiance across a selection of typical flame configurations. This approach is significant in that it yields good accuracy without the need for spectral integration.

The differential total absorptivity solution is similar to TTNH in that it is based on differential total properties. However, it differs with respect to its explicit treatment of the source temperature dependence of absorption. Therefore, the DTA solution avoids the corrections required by TTNH. Both methods are less computationally expensive than the banded solutions, but are more expensive than the **weighted-sum-of-gray-gases** solution (WSGG). Some authors [16] and [17] have generated WSGG coefficients for gas-soot mixtures. Modest [18] has demonstrated good accuracy of the WSGG concept in the **P-1** approximation to radiative transfer in black-walled enclosures.

The ultimate goal of linking the predictive techniques described above in computational fluid dynamics (CFD) combustion calculations is attracting increasing levels of interest. Until recently, many researchers have represented radiative loss from **nonpremixed** flames in the laminar **flamelet** combustion model by perturbing an adiabatic temperature flamelet by a fixed fraction. Syed et al. [19] adopted this approach in developing their soot **model**, and then postprocessed the concentration and temperature fields in a spectral **line-of-sight-radiation** calculation. Similarly, Fairweather et al. [9] decoupled radiation from the energy equation and applied their converged solution to a DTRM calculation to predict the radiation received external to a turbulent reacting jet in a cross wind. They used a large number of rays (1,024) and the narrow-band property model. In contrast, **Bhattacharjee** and Grosshandler [20] performed a parabolic analysis of a nonpremixed methane flame with the effective **angle/TTNH** model coupled to a steady-state soot model. Kent and **Honnery** [21] and **Kaplan** et al. [22] have coupled radiative loss to the energy **equation—and** to soot formation **processes—using the** discrete-ordinates radiation model but with simplified expressions for the absorption coefficient. In view of these advances in modeling techniques, and with the continual expansion in computing power, it is becoming increasingly feasible to perform coupled radiation combustion product distribution calculations in three-dimensional CFD codes. The DTA solution provides a powerful means by which calculated concentrations and **thermodynamic** properties can be **applied** in the discrete transfer radiation model to evaluate the transfer of energy by radiation.

Initially, the DTA solution is assessed across **line-of-sight** soot profiles in the absence of  $\text{CO}_2$  and  $\text{H}_2\text{O}$ . The soot volume fraction (and temperature) **profiles** are symmetrical parabolic maxima and minima in the range  $0.6\text{e-}7$  to  $1.6\text{e-}7$  (800 to 1,800 K). Then the same profiles are analyzed with the addition of  $\text{CO}_2$  and  $\text{H}_2\text{O}$  in the ratio 1:2. Finally, both configurations are adopted in a DTRM calculation between solid **walls** at the same temperature as the adjacent mixture. Both black and **low-emissivity** ( $e = 0.25$ ) walls are considered.

In **all** comparisons, a benchmark is provided by the DBT solution, which is based on the computer code **RADCAL**, described by **Grosshandler** [23].

An additional feature of this article is an enhancement to the treatment of reflection in **the** total property solutions. This addresses the fact that reflected radiation from **nonuniform** paths originates from temperatures different from the wall temperature.

## THEORY

The discrete transfer radiation model is a ray-tracing procedure that iteratively solves the radiative flux at solid boundaries. **Rays** are traced from computational cell wall boundaries in discrete directions, and the radiative transfer equation is solved along each path. Therefore, radiative fluxes are evaluated by a summation of individual line-of-sight solutions to the **RTE** [5, 6]. Hence, it is possible to assess initially the feasibility of a solution procedure for the DTRM by evaluating its accuracy when applied to a single line of sight.

### Modeling of the RTE for Soot

Before **considering** the radiative intensity across paths of gas-soot mixtures, it is appropriate to address the treatment of soot radiation in isolation. From the Mie theory, the size parameter,  $\pi D/\lambda$ , where  $D$  is the particle diameter, is sufficiently small in typical combustion systems to neglect scattering. Thus, since the attenuation of radiation by soot is known to obey Bouger's law [7], the variation of a soot absorption coefficient is required for the determination of radiation intensity along a path.

The absorption coefficient of soot is a complicated function of fuel type, of fuel and **oxidant** mixing, and of flame geometry and temperature. Additionally, its variation with wavelength differs among fuels. However, many experimentally determined empirical relations **reveal** that the absorption coefficient is directly proportional to soot volume fraction, and that an inverse relation exists between the absorption coefficient and wavelength [7]. These relationships are summarized by

$$k = c_0 \Phi \lambda^{-\beta} \quad (1)$$

where, for a particular fuel,  $\beta$  is represented by a mean value, by a logarithmic function of wavelength, or by a polynomial function of wavelength. A detailed description of these dependencies is given by Siegel and Howell [7]. The dimension-

less constant,  $c_0$ , is determined from the optical properties of soot,

$$c_0 = \frac{36\pi n x}{(n^2 - x^2 + 2)^2 + 4n^2 x^2} \quad (2)$$

where  $n$  and  $x$  are the refractive index and extinction coefficient, respectively. For a given field of soot volume fraction, the solution of the RTE for soot is significantly simplified if  $\beta$  is assumed to be a constant value equal to unity, and if both the refractive index and the extinction coefficient are assumed to be weak functions of wavelength. These are not unreasonable assumptions to make for soot particles that are small relative to the wavelength of radiation [15]. A value of 7.0 for  $c_0$ , justified in [15], is employed here.

Having formulated an expression for the absorption coefficient, it is possible to derive solutions to the radiative transfer equation. Using the differential absorptivity form of the RTE, the intensity across a path with cold black boundaries is

$$i(s) = - \int_0^\infty \int_0^s i_{\nu}(s') \frac{\delta \alpha_{\nu}(s' \rightarrow s)}{\delta s'} ds' d\nu \quad (3)$$

A direct solution to this equation for soot is obtained if Eq. (1) and the Planck function,

$$i_b(T, \nu) = \frac{2C_1 \nu^5}{e^{C_2 \nu/T} - 1} \quad (4)$$

are substituted into Eq. (3), yielding

$$i_p = - \frac{c_0 C_1}{\pi C_2^5} \int_0^s \left[ T(s')^5 \Phi(s') \Psi^{(4)} \left( 1 + \frac{c_0 T(s')}{C_2} \int_{s'}^s \Phi(s'') ds'' \right) \right] ds' \quad (5)$$

The hexa-gamma function,  $\Psi^4$ , is solved using the series expansion

$$\Psi^n(z) = (-1)^{n+1} n! \sum_{k=0}^{\infty} (z+k)^{-n-1} \quad (6)$$

from Abramowitz and Stegun [24]. Representing Eq. (5) numerically across  $m$  elements yields a direct solution to the RTE for soot,

$$i_{n,p} = - \frac{c_0 C_1}{\pi C_2^5} \sum_{n=1}^N I \left[ T_n^5 \Phi_n \Psi^{(4)} \left( 1 + \frac{c_0 T_n}{C_2} \sum_{n'=n}^N I(\Phi_{n'}, \Delta s_{n'}) \right), \Delta s_n \right] \quad (7)$$

where  $I(a, b)$  represent individual terms in the numerical integration. This direct solution to Eq. (3) can now be compared to solution techniques based on the discretization of the absorptivity differential in Eq. (3) as described in [5].

In the differential banded transmissivity (DBT) solution,

$$i_n = \sum_{j=1}^J \left[ \sum_{r=1}^n \bar{i}_b(T_s, \nu_j) (\bar{\tau}_{r \rightarrow n, j} - \bar{\tau}_{r-1 \rightarrow n, j}) \Delta \nu_j \right] \quad (8)$$

the soot transmissivity for a narrow band from the leading edge of a cell to the end of the path is

$$\bar{\tau}_{p, r \rightarrow n, j} = e^{-c_0 \Phi \nu L} \quad (9)$$

where  $\nu$  is the wave number at the center of a band and  $L$  is the distance  $r \rightarrow n$ . For inhomogeneous paths a mean value of soot volume fraction is required.

The differential total absorptivity solution applied to gas radiation used Modak's total property curve-fitting strategy [14] for  $\text{CO}_2$  and  $\text{H}_2\text{O}$ . It is based on the definition of total absorptivity as

$$\alpha^T = \frac{\int_0^\infty i_b(T, \nu) \alpha(T, \nu) d\nu}{\int_0^\infty i_b(T, \nu) d\nu} \quad (10)$$

Discretization of the differential absorptivity in Eq. (3) yields terms such as the numerator in Eq. (10). Hence, the **integro-differential RTE** in Eq. (3) reduces to a path summation of total absorptivity differences. When applied to soot, the DTA solution becomes

$$i_{n,p} = \sum_{r=1}^n i_b(T_{r-1/2}) \left[ \alpha_{r-1 \rightarrow n}^T(T_{r-1/2}, \bar{\Phi}_{r-1 \rightarrow n}, l_{r-1 \rightarrow n}) - \alpha_{r \rightarrow n}^T(T_{r-1/2}, \bar{\Phi}_{r \rightarrow n}, l_{r \rightarrow n}) \right] \quad (11)$$

The **absorptivities** in Eq. (11) are functions of the distribution of soot and of the source temperature. In contrast to the curve-fitting methods adopted for  $\text{CO}_2$  and  $\text{H}_2\text{O}$ , accurate and relatively simple analytical expressions are available for soot.

When Eq. (1) with  $\beta$  equal to unity, and Eq. (4) are substituted into Eq. (10), the total absorptivity of soot across a path from  $s'$  to  $s$  is

$$\alpha^T(s' \rightarrow s) = 1 - \frac{15}{\pi^4} \Psi^{(3)} \left[ 1 + \frac{c_0 T(s')}{C_2} \int_{s'}^s \Phi(s'') ds'' \right] \quad (12)$$

The penta-gamma function  $\Psi^{(3)}$  is evaluated by the poly-gamma series expansion, Eq. (6), and the integral is treated as it is in Eq. (7).

Alternatively, if  $e^{c_2 \nu / T} \gg 1$  in Eq. (4), Wien's treatment of the blackbody intensity yields

$$\alpha^T(s' \rightarrow s) = 1 - \left[ \frac{1 + c_0 \bar{\Phi} L T(s')}{C_2} \right]^{-4} \quad (13)$$

as an approximation to Eq. (12) [7]. The mean value of soot volume fraction is evaluated from  $s'$  to  $s$ .

Other authors have simplified the absorptivity further by assuming soot radiation to be gray [25]. The dependence on temperature and soot distribution is then carried by an absorption coefficient such that

$$\alpha^T(s' \rightarrow s) = 1 - \exp\left[-\frac{C_0 \bar{\Phi} L T(s')}{C_2}\right] \quad (14)$$

Suitable values for the constant  $C$  are obtained by substituting Eq. (1) into expressions for a mean absorption coefficient. The Rosseland mean in the optically thick limit yields a value of 3.6. Yuen and Tien [25] recommended this value in evaluating the total emissivity from a range of luminous flames. More recently, Kent and Honnery [21] adopted the Planck mean absorption coefficient in the optically thin limit ( $C = 3.827$ ) in the analysis of a laminar ethylene flame. The higher value for  $C$  is used in the present article because initial results yielded better predictions than the lower value.

A number of authors have incorporated the emissivity of soot into the **weighted-sum-of-gray-gases** (WSGG) model. The most straightforward representation, exemplified by Truelove [16], manipulates the coefficients for soot and gases alone into a single expression of the form

$$\varepsilon = \sum_{n,n'} a_{m,n,n'}(T) \left\{ 1 - \exp\left[-k_{g,n}(p_h + p_c) - k_{p,n'} \rho_p \Phi\right] L \right\} \quad (15)$$

The temperature polynomial coefficients are such that Eq. (15) reduces to the soot-free and soot-dominant limits.

Finally, the **most** straightforward treatment of the RTE path integral is afforded by a constant-absorption-coefficient (CAC) gray gas approximation. Although the simplification is attractive computationally, and notwithstanding the possibility of generating reasonable accuracy along certain paths, a single value is **unlikely** to yield acceptable accuracy throughout a domain. Additionally, the best representative value is not known in advance of calculation.

For further details concerning the different solution techniques and their implementation in the **DTRM**, the reader is referred to Bressloff et al. [5]. Table 1 summarizes the main solutions included in the comparisons presented below.

When a low soot concentration is combined with  $\text{CO}_2$  and  $\text{H}_2\text{O}$ , the overall radiative behavior maintains the nongray characteristics of the gaseous compo-

**Table 1.** Solution methods

DBT	Differential banded <b>transmissivity</b> solution using the narrow-band model due to Ludwig et al. [8]
DTA	Differential total absorptivity solution using Modak's total emissivity data [14] for gases and Eq. (12) or (14) for soot
WSGG	Weighted-sum-of-gray-gases solution using Truelove's coefficients [16]
CAC	Constant-absorption-coefficient solution

nents, the mixture being dominated by the gases. Similarly, when a high soot loading is imposed on the gas mixture, the soot characteristics are more prominent. However, there is an intermediate range of soot loading in which neither component dominates and the effects of both gas and soot must be accounted for. Under a variety of uniform conditions, Felske and Tien [12] identified this range to be approximately centered at a value of  $\Phi L = 10^{-7}$  m. In order to encompass this range within the **inhomogeneous** configurations analyzed below, parabolic profiles of soot volume fraction are adopted varying between  $0.6e-7$  and  $1.6e-7$  for a total path length of 1 m.

### Line-of-Sight Predictions Across Soot (without Gases)

An assessment of the DTA solution applied to soot is presented in Figures 1 and 2. The DTA solution, with total absorptivity evaluated from Eq. (12) and from Eq. (14), is compared to the direct solution for soot intensity represented by Eq. (7), the DBT solution, and the WSGG solution. Also shown are CAC solutions across a range of absorption coefficients.

In Figure 1 the variation of radiative intensity is shown across a line of sight represented by configuration A:

$$T = 800.0[5.0s(1.0 - s) + 1.0] \quad (16)$$

$$\Phi = [40.0s(1.0 - s) + 6.0] \times 10^{-8}$$

The intensity increases through a point of inflection to a maximum close to the end of the line of sight. There are negligible differences among the narrow-band DBT

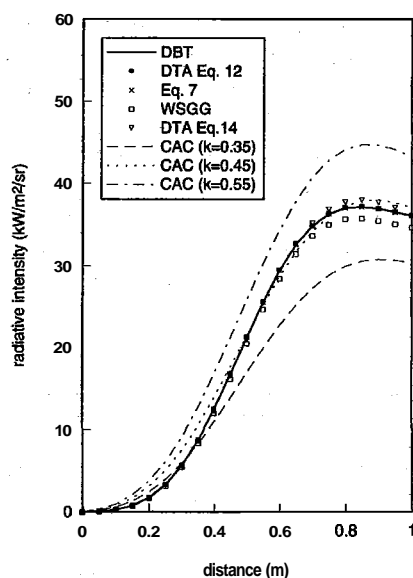


Figure 1. Radiative intensity across configuration A for soot without gases.

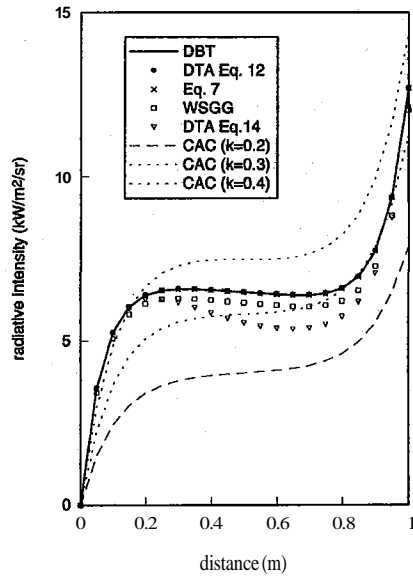


Figure 2. Radiative intensity across configuration **B** for soot without gases.

solution, the direct solution, and the DTA solution using the **closed-form** expression—Eq. (12)—for total absorptivity. The DTA method employing Eq. (14), however, **overpredicts** intensity in the vicinity of the maximum. The WSGG solution **underpredicts** intensity with a mean percentage error of 4.52%, evaluated from

$$E = 100 \sum_{n=1}^N \frac{|I_{\text{DBT},n} - I_n|}{N} \quad (17)$$

where  $I$  represents radiative intensity (or volumetric radiative sources in the DTRM calculations).

The intensity variation across configuration B, represented by

$$\begin{aligned} T &= 200.0[20.0s(s - 1.0) + 9.0] \\ \Phi &= [4.0s(s - 1.0) + 1.6] \times 10^{-7} \end{aligned} \quad (18)$$

is shown in Figure 2. In this case, the relatively high temperature and concentration of soot at the start of the path emit quite powerfully. However, a point is reached whereby the cooler, less dense region cannot emit more than it absorbs and the profile flattens to an almost constant intensity. Eventually, there is a rapid increase in emission at the hotter, high-concentration end of the path.

Again, there are **almost** indiscernible differences among the direct, DBT, and DTA solutions. However, larger errors are observed for the WSGG solution and the DTA solution using Eq. (14), with both methods **underpredicting** intensity.

There has been some uncertainty concerning the temperature to use in Eq. (14) for the DTA solution. In the closed-form expression of Eq. (12) the temperature dependence is due to the source and not the subsequent path. This suggests

that the source temperature should be applied in Eq. (14). However, considerable deviation of intensity exists in these cases, especially for configuration B, in which an error of almost 100% occurs 0.8 m from the origin. When the mean path temperature is used, the error is reduced considerably. Therefore, all results for the DTA solution employing Eq. (14) use the mean path temperature.

Despite the nongray formulation in Eq. (1), Markstein [13] has demonstrated that the single-gray-gas approximation becomes an increasingly good approximation of soot radiation as soot concentration increases. Therefore, it is not surprising that solution to the RTE with a constant absorption coefficient, CAC, should yield greater accuracy for the intensity profiles due to soot radiation alone compared to those for gases in the absence of soot. In Figure 1 an absorption coefficient of 0.45 captures the intensity variation very well. The profile is not captured as accurately in Figure 2, but a value between 0.3 and 0.4 locates the position of the profile. This accuracy is in contrast to the observations made by Bressloff et al. [5] for the CAC predictions of intensity for CO<sub>2</sub>-H<sub>2</sub>O mixtures.

### Mixtures of Soot, CO<sub>2</sub>, and H<sub>2</sub>O

The treatment of soot radiation described above is now combined with that for CO<sub>2</sub>-H<sub>2</sub>O mixtures.

In the differential banded transmissivity solution the transmissivity is evaluated as the product of all component transmissivities. However, it is less straightforward to combine the direct solution to soot intensity, Eq. (7), with approximations for gaseous radiation, since it is not possible to add the two contributions linearly. When the spectral absorptivity is expanded for each mixture component,

$$\alpha_{\nu, g+p} = \alpha_{\nu, g} + \alpha_{\nu, p} - \alpha_{\nu, g} \alpha_{\nu, p} \quad (19)$$

Substituting Eq. (19) into Eq. (3) then yields the total intensity as the sum of the intensities solved separately for the solid and gaseous states together with a correction. This approach has been applied in [15] using TNH for gaseous radiation, Eq. (7) for particulate radiation, and an iterated temperature term for the correction. Grosshandler and Modak [15] identified weaknesses of this method for certain paths. They suggested that for some configurations it was preferable to add the gas radiance to a term representing soot radiance that is transmitted by the gas. A further alternative is to write the combined absorptivity from Eq. (19) as

$$\alpha_{\nu, g+p} = \alpha_{\nu, p} + \alpha_{\nu, g} \tau_{\nu, p} \quad (20)$$

In this form, gas radiance transmitted by the soot is added to the radiance due to soot alone. Thus, if

$$\alpha_{s'p}^{T_s T} = \frac{\int_0^\infty i_b(T_s, \nu) \alpha_{\nu, g} \tau_{\nu, p} d\nu}{\int_0^\infty i_b(T_s, \nu) d\nu} \quad (21)$$

then the radiative intensity is

$$i_n = i_{n,p} + \sum_{r=1}^n i_b(T_{r-1/2}) (\alpha_{g,r \rightarrow n-1}^T \tau_{p,r \rightarrow n-1}^T - \alpha_{g,r \rightarrow n}^T \tau_{p,r \rightarrow n}^T) \quad (22)$$

where  $i$  is given by Eq. (7). This representation is preferred in the present context because the **transmissivity** of soot can then be based on the source temperature of each differential path. Additionally, it avoids the need to evaluate an equivalent temperature for the overlap correction term [15]. The gaseous total **absorptivities** can be calculated by the methods described in [5], and the total soot transmissivity can be calculated from any of Eqs. (12)-(14).

Solution of the RTE based on Eq. (20) has also been **applied** extensively with the exponential wide-band model for gaseous radiation [14, 26].

The feasibility of expressing the second term of Eq. (20) in terms of the product of total radiative properties suggests that it should be possible to extend the differential total absorptivity solution to mixtures of soot and gases. So, from the definition

$$\tau_g^T \tau_p^T = \frac{\int_0^\infty i_b(T_s, \nu) \tau_{v,g} \tau_{v,p} d\nu}{\int_0^\infty i_b(T_s, \nu) d\nu} \quad (23)$$

the DTA solution for gas-soot mixtures becomes

$$i_n = \sum_{r=1}^n i_b(T_{r-1/2}) (\tau_{g,r \rightarrow n}^T \tau_{p,r \rightarrow n}^T - \tau_{g,r \rightarrow n-1}^T \tau_{p,r \rightarrow n-1}^T) \quad (24)$$

in which transmissivities are evaluated from source temperature-dependent absorptivities. Hence, the transmissivity products are treated on a total basis from the leading and trailing edges of elements and summed for all elements in a path.

The preceding analysis has not included radiation from solid boundaries. In the DBT and WSGG solutions, the presence of soot does not alter the treatment for **solid-wall** radiation described in [5]. However, in the differential total property solutions, consideration is required of the total transmissivity of wall radiation. Here, the soot transmissivity is extracted from the product of spectral transmissivities to again yield a product of total transmissivities. The transmission of solid wall radiation is then  $i_0 \tau_g \tau_p$ .

A problem with this method has been encountered, however, especially with high-reflectivity cool **walls** bounding a hot gas. It would seem that using the relatively low wall temperature to **evaluate** the absorptivity of radiation, part of which originates at a higher temperature, leads to an underestimation of overall absorption. An effective wall temperature,

$$T_w' = \left\{ \frac{\pi}{\varepsilon \sigma} \left[ \frac{\varepsilon \sigma T_w^4}{\pi} + (1 - \varepsilon) q^- \right] \right\}^{0.25} \quad (25)$$

is therefore employed in the calculation of total absorptivities such that the wall is assumed to be radiating as a blackbody at this temperature.

## DISCUSSION OF RESULTS

### Single Lines of Sight

In Figures 3 and 4 the same comparisons for a gas-soot mixture are made as those for soot alone.  $\text{CO}_2$  and  $\text{H}_2\text{O}$  are in the ratio 1:2. Also shown in Figure 3 are the contributions due to the separate components. Although the gaseous contribution is the more dominant for the bulk of the path, the radiance at the end of the path is greatest for the soot. Both contributions are of the same order of magnitude.

Relative to the DBT solution, both DTA solutions have a mean percentage error of less than 7%. They also agree very closely with each other, this being the consequence of a reduced significance of error from Eq. (14) when used for the gas-soot mixture. The WSGG solution and the modified Grosshandler method, Eq. (22), show greater deviation from the DBT solution, especially at the end of the line of sight, where there are absolute errors of 13.37% and 19.30%, respectively. The errors are summarized in Table 2. The overall mean percentage error of the modified Grosshandler method compares favorably with that for the DTA solution due to lower absolute errors at shorter path lengths.

The intensity variation across configuration B is shown in Figure 4. The contribution due to the gas varies between two and three times that due to the soot. Hence, the central region of the profile mirrors the strong absorption of the

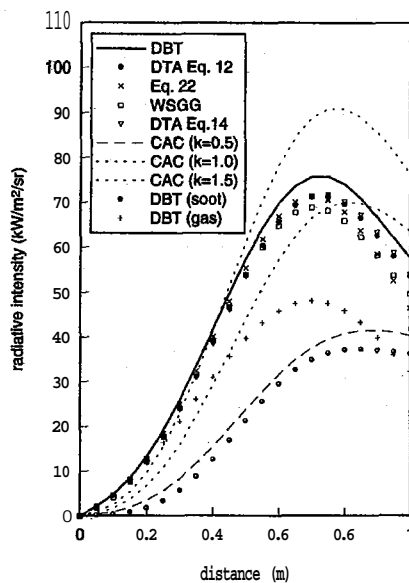


Figure 3. Radiative intensity across configuration A for  $\text{CO}_2$ - $\text{H}_2\text{O}$ -soot mixture.

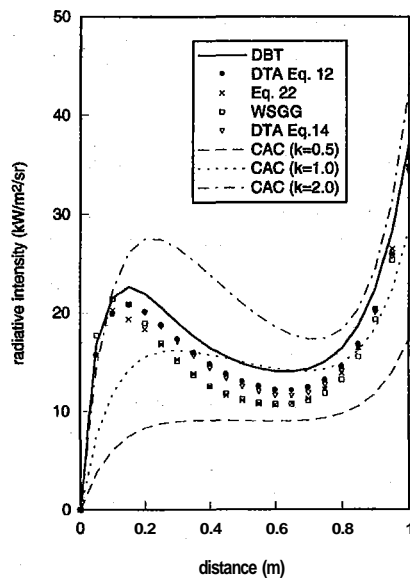


Figure 4. Radiative intensity across configuration B for  $\text{CO}_2\text{-H}_2\text{O}$ -soot mixture.

relatively cool gas. All solutions **overpredict** absorption across the whole line of sight, with the lowest mean percentage error provided by the DTA solution using Eq. (12).

A representative CAC solution is given by an absorption coefficient close to unity for both configurations. The errors are approximately 27% and 16%, respectively. Notwithstanding the attraction of the CAC solution in terms of computational effort, it is to be recalled that a suitable absorption coefficient is determined by trial and error and the full shape of the profile is not captured.

Having assessed the DTA solution across single lines of sight, it is now applied in a **DTRM** calculation across the same configurations and between solid walls of high and low **emissivity**. The volumetric radiative source term for a cell is

Table 2. Mean absolute percentage errors relative to the DBT solution

	DTA Eq. (12)	DTA Eq. (14)	Eq. (22)	WSGG
A, line of sight	6.42	6.34	6.63	9.78
B, line of sight	10.09	12.04	16.77	17.04
A, solid wall ( $e = 1.0$ )	6.22	4.52	<b>6.93</b>	8.79
A, solid wall ( $e = 0.25$ )	1.82	4.25	3.17	6.87
B, solid wall ( $e = 1.0$ )	2.94	17.44	<b>8.00</b>	3.97
B, solid wall ( $e = 0.25$ )	6.33	5.52	6.76	3.83

evaluated by summing, for each ray that crosses the cell, the intensity change scaled by a solid-angle weighting factor and the projected area of the boundary from which the ray originates [5].

#### DTRM Calculation across Configuration A between Solid Walls

For configuration A with walls at 800 K, the hot mixture is a net emitter of radiation. The relatively cool edges, however, absorb a proportion of this energy before it arrives at the walls. This energy exchange yields the radiative source variation shown for high-emissivity walls ( $e = 1.0$ ), Figure 5, and for low-emissivity walls ( $s = 0.25$ ), Figure 6. In the latter case there is greater absorption by the cool edges, since a large fraction of radiation from the hot mixture is reflected at the walls. For the black walls, all of the mixture radiance is absorbed by the walls.

With reference to Table 2, all methods demonstrate good accuracy, with the lowest error accompanying the DTA solution. There is a slight loss of performance for all solutions at the center of the black wall profile, and the WSGG solution loses accuracy at the edges in Figure 6.

For the CAC solutions, an absorption coefficient of 0.9 has an error of 9.13% between black walls, but the source variation is less well predicted by an absorption coefficient of unity for the low-emissivity walls (error = 14.91%).

#### DTRM Calculation across Configuration B between Solid Walls

When configuration B is applied between walls at 1,800 K, the mixture becomes an overall absorber. The greatest net absorption occurs approximately one-fifth of the distance from each wall, thus generating the M-shaped radiative source variation shown in Figures 7 and 8. In the black wall case, only a small region of the mixture adjacent to the walls emits more radiation than it absorbs. This region expands for the mixture between gray walls, and the absolute value of this loss increases due to the low emissivity of the walls.

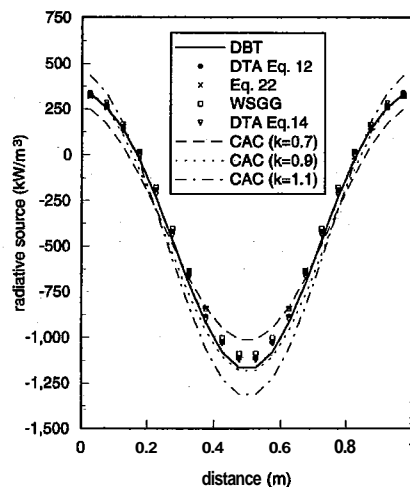


Figure 5. Radiative source across configuration A bounded by solid walls (emissivity = 1.0) for  $\text{CO}_2\text{-H}_2\text{O-soot}$  mixture.

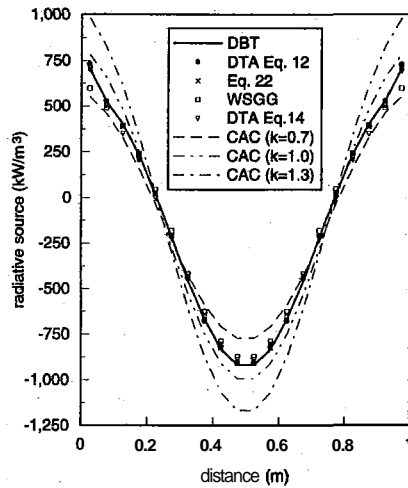


Figure 6. Radiative source across configuration A bounded by solid walls (emissivity = 0.25) for  $\text{CO}_2\text{-H}_2\text{O}$ -soot mixture.

The DTA solution using Eq. (12) has the lowest mean percentage error in both cases, although a local error of approximately 14% occurs adjacent to the gray walls. This is most likely due to the effective wall temperature calculated by Eq. (25) exceeding, and, therefore, approximated to the 2,000 K limit of Modak's gas absorptivity calculation.

The other solution techniques appear to have difficulty predicting the absorption of radiation from the high-temperature, black walls. The modified Grosshandler method and the second DTA solution both underestimate net absorption, whereas the WSGG solution overpredicts the balance between absorption and emission in the center of the slab. The worst performance is produced by the second DTA solution, with a mean percentage error of 17.44%; however, the use of the optically thin assumption for soot in the DTA solution is not expected to encompass all configurations.

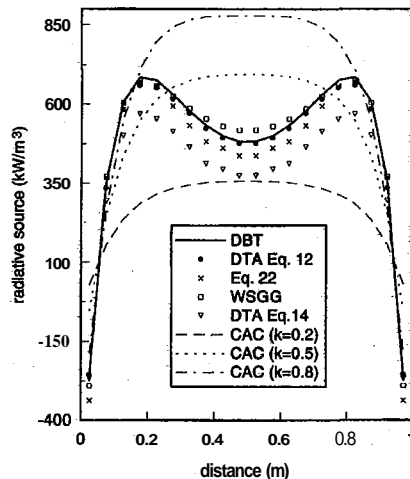
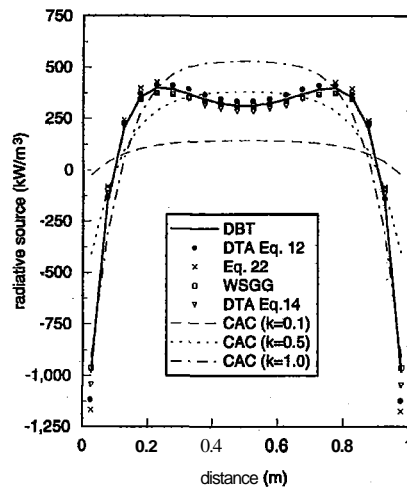


Figure 7. Radiative source across configuration B bounded by solid walls (emissivity = 1.0) for  $\text{CO}_2\text{-H}_2\text{O}$ -soot mixture.



**Figure 8.** Radiative source across configuration B bounded by solid walls (emissivity = 0.25) for  $\text{CO}_2\text{-H}_2\text{O}$ -soot mixture.

In both black and gray wall configurations, an absorption coefficient of approximately 0.5 locates the level of the source variation, **but** the CAC solution fails to capture **the** M-shaped profile.

### CONCLUSIONS

The differential total absorptivity solution has been applied **successfully** to mixtures of **soot**,  $\text{CO}_2$ , and  $\text{H}_2\text{O}$  across individual lines of sight and in a complete discrete transfer radiation model calculation **between** solid boundaries. Consequently, explicit treatment of the source temperature dependence of absorption has been demonstrated for gas-soot mixtures without the need for spectral integration.

Predictions have been favorable for both **black** and gray walls. In all the DTRM calculations, the DTA solution has mean percentage errors below 7% and lower than the modified Grosshandler solution and the WSGG solution. When the mixture is modeled as a single gray gas with a fixed absorption coefficient, it is possible to predict individual **line-of-sight** intensity variations reasonably well. However, the best value is ascertained only by trial and error. Therefore, in a DTRM calculation the volumetric radiative source variation can be poorly represented.

Computationally, the DTA solution, and the modified Grosshandler method are over two orders of magnitude faster than the narrow-band DBT solution. However, the WSGG solution is over an order of magnitude faster than the total property solutions.

If the additional tune penalty of the DTA solution relative to the WSGG solution is too severe in a fully coupled **radiation-CFD-combustion** calculation, it is possible to start radiation predictions using the WSGG solution and then replace it with the DTA solution later in convergence. Such an approach then yields the additional accuracy accompanying the DTA solution without incurring excessive computational expense.

The DTA solution is currently being assessed in CFD simulations of turbulent diffusion flames, both buoyancy and convection dominated, both confined and **unconfined**. The radiation predictions are fully coupled to the energy equation and to soot formation models, thus emphasizing **the** current state of the art in computational combustion modeling.

#### REFERENCES

1. F. C. **Lockwood** and W. M. G. Malalasekera, Fire Computation: The "Flashover" Phenomenon, *Twenty-Second Symp. (Int.) on Combustion*, pp. 1319-1328, The Combustion Institute, Pittsburgh, PA, 1988.
2. M. A. Delichatsios and L. **Orloff**, Effects on Turbulence of Flame Radiation from Diffusion Flames, *Twenty-Second Symp. (Int.) on Combustion*, pp. 1271-1279, The Combustion Institute, Pittsburgh, PA, 1988.
3. K. K. Kuo, *Principles of Combustion*, p. 516, John **Wiley**, New York, 1986.
4. **Bockhorn**, H. (ed.), *Soot Formation in Combustion (Mechanisms and Models)*, Springer Series in Chemical Physics 59, **Springer-Verlag**, Berlin, 1994.
5. N. W. **Bressloff**, J. B. Moss, and P. A. **Rubini**, Assessment of a Differential Total Absorptivity Solution to the Radiative Transfer Equation as Applied in the Discrete Transfer Radiation Model, *Numer. Heat Transfer, Part B*, vol. 29, no. 3, pp. 381-397, 1996.
6. F. C. Lockwood and N. G. Shah, A New Radiation Solution Method for Incorporation in General Combustion Prediction Procedures, *Eighteenth Symp. (Int.) on Combustion*, pp. 1405-1414, The Combustion Institute, Pittsburgh, PA, 1981.
7. R. Siegel and J. R. Howell, *Thermal Radiation Heat Transfer*, pp. 653-673, Hemisphere, Washington, DC, 1992.
8. C. B. Ludwig, W. **Malkmus**, J. E. Reardon, and J. A. L. Thomson, *Handbook of Infrared Radiation from Combustion Gases*, **NASA SP-3080**, Scientific and Technical Information Office, Washington, DC, 1973.
9. M. **Fairweather**, W. P. Jones, and R. P. Lindstedt, Predictions of Radiative Transfer from a Turbulent Reacting Jet in a **Cross-Wind**, *Combustion & Flame*, vol. 89, pp. 45-63, 1992.
10. D. K. Edwards, Molecular Gas Band Radiation, in *Advances in Heat Transfer, Vol. 12*, pp. 115-193, Academic Press, New York, 1976.
11. P. **Docherty** and M. Fairweather, Predictions of Radiative Transfer from Nonhomogeneous Combustion Products Using the Discrete Transfer Method, *Combustion & Flame*, vol. 71, pp. 79-87, 1988.
12. J. D. Felske and C. L. Tien, Calculation of the **Emissivity** of Luminous Flames, *Combustion Sci. Technol.*, vol. 7, pp. 25-31, 1973.
13. G. H. **Markstein**, Radiative Energy Transfer from Gaseous Diffusion Flames, *Fifteenth Symp. (Int.) on Combustion*, pp. 1285-1294, The Combustion Institute, Pittsburgh, PA, 1974.
14. A. T. Modak, Radiation from Products of Combustion, *Fire Res.* vol. 1, pp. 339-361, 1979.
15. W. L. **Grosshandler** and A. T. Modak, Radiation from **Nonhomogeneous** Combustion Products, *Eighteenth Symp. (Int.) on Combustion*, pp. 601-609, The Combustion Institute, Pittsburgh, PA, 1981.
16. J. S. **Truelove**, Zone Method for Radiative Heat Transfer Calculations, **HTFS DR33**, AERE, Harwell, Oxon, England, 1975.
17. J. D. Felske and T. T. Charalampopoulos, Gray Gas Weighting Coefficients for Arbitrary Gas-Soot Mixtures, *Int. J. Heat Mass Transfer*, vol. 25, no. 12, pp. 1849-1855, 1982.

18. M. F. Modest, The **Weighted-Sum-of-Gray-Gases** Model for Arbitrary Solution Methods in Radiative Transfer, *J. Heat Transfer*, vol. 113, pp. 650-656, 1991.
19. K. J. Syed, C. D. **Stewart**, and J. B. Moss, Modelling Soot Formation and Thermal Radiation in Buoyant Turbulent Diffusion Flames, *Twenty-Third Symp. (Int.) on Combustion*, pp. 1533-1541, The Combustion Institute, Pittsburgh, PA, 1990.
20. S. **Bhattacharjee** and W. L. Grosshandler, Effect of Radiative Heat Transfer on Combustion Chamber Flows, *Combustion & Flame*, vol. 77, pp. 347-357, 1989.
21. J. H. **Kent** and D. R. **Honnery**, A Soot Formation Map for a Laminar Ethylene Diffusion Flame, *Combustion & Flame*, vol. 79, pp. 287-298, 1990.
22. C. R. **Kaplan**, S. W. **Baek**, E. S. Oran, and J. L. **Ellzey**, Dynamics of a Strongly Radiating Unsteady Ethylene Jet Diffusion Flame, *Combustion & Flame*, vol. 96, pp. 1-21, 1994.
23. W. L. Grosshandler, Radiative Heat Transfer in **Nonhomogeneous** Gases: A Simplified Approach, *Int. J. Heat Mass Transfer*, vol. 23, pp. 1447-1459.
24. M. **Abramowitz** and I. A. **Stegun**, *Handbook of Mathematical Functions*, Eq. 6.4.10, p. 260, Dover, New York, 1972.
25. W. W. Yuen and C. L. Tien, A Simple Calculation Scheme for the **Luminous-Flame Emissivity**, *Sixteenth Symp. (Int.) on Combustion*, pp. 1481-1487, The Combustion Institute, Pittsburgh, PA, 1976.
26. R. O. Buckius and C. L. Tien, Infrared Flame Radiation, *Int. J. Heat Mass Transfer*, vol. 20, pp. 93-106, 1977.